Plasma Sheet Source and Loss Processes

Technical Report in Lieu of Performance Report
on Grant No. NAG5-7463

covering the period
January 1 through December 31, 1999

Principal Investigator
O.W. Lennartsson

Lockheed Martin Missiles & Space, ATC
Org. L9-42, Building 255
3251 Hanover Street
Palo Alto, CA 94304

The attached document, entitled **Polar/TIMAS survey of earthward field-aligned proton flows from the near-midnight tail**, reports on the first year of research under subject grant. This report has just been completed and will be submitted for publication in the *Journal of Geophysical Research.*

Walter Lennartsson

O.W. Lennartsson
Principal Investigator

To be submitted to
the Journal of Geophysical Research, January, 2000

Polar/TIMAS survey of earthward field-aligned proton flows from the near-midnight tail

O.W. Lennartsson, K.J. Trattner, H.L. Collin and W.K. Peterson

All at Lockheed Martin Missiles & Space, ATC, 3251 Hanover St., Palo Alto, CA 94304, USA

Abstract. Data from the TIMAS ion mass spectrometer on the Polar satellite, covering 15 eV/*e* to 33 keV/*e* in energy and essentially 4π in view angles, are used to investigate the properties of earthward (sunward) field-aligned flows of ions, especially protons, in the plasma sheet-lobe transition region near local midnight. A total of 142 crossings of this region are analyzed at 12-sec time resolution, all in the northern hemisphere, at R(SM) ~ 4-7 R_E, and most (106) in the poleward (sunward) direction. Earthward proton flows are prominent in this transition region (> 50% of the time), typically appearing as sudden "blasts" with the most energetic protons (~33 keV) arriving first with weak flux, followed by protons of decreasing energy and increasing flux until either (1) a new "blast" appears, (2) the flux ends at a sharp boundary, or (3) the flux fades away within a few minutes as the mean energy drops to a few keV. Frequent step-like changes (<12 sec) of the flux suggest that perpendicular gradients on the scale of proton gyroradii are common. Peak flux is similar to central plasma sheet proton flux (10^5–10^6 [cm^2 sr sec keV/*e*]$^{-1}$) and usually occurs at E ~ 4-12 keV. Only the initial phase of each "blast" (~1 min) displays pronounced field-alignment of the proton velocity distribution, consistent with the time-of-flight separation of a more or less isotropic source distribution with $df/dv < 0$. The dispersive signatures are often consistent with a source at R(SM) ≤ 30 R_E. No systematic latitudinal velocity dispersion is found, implying that the equatorial plasma source is itself convecting. In short, the proton "blasts" appear as sudden local expansions of central plasma sheet particles along reconfigured ("dipolarized") magnetic field lines.

1. Introduction

Magnetic field-aligned flows of energetic (up to several tens of keV) ions, usually assumed to be protons, from the deep tail toward Earth have been reported from many experiments, initially from instruments on polar orbiting satellites [*Hultqvist et al.*, 1971] but later and much more extensively from instruments flown in near-equatorial orbits well downtail [e.g. *Lui et al.*,1977; *DeCoster and Frank*, 1979; *Parks et al.*, 1979 and 1984; *Krimigis and Sarris*, 1980; *Spjeldvik and Fritz*,1981; *Williams*, 1981; *Lyons and Speiser*, 1982; *Eastman et al.*, 1985; *Onsager et al.*, 1991; *Paterson et al.*, 1998; *Lyons et al.*, 1999]. With their presence well established by tail observations and their study facilitated by continued improvements in detector time resolution, these flows have come under increasing scrutiny by near-Earth high-latitude observations as well [e.g. *Zelenyi et al.*, 1990; *Saito et al.*, 1992; *Bosqued et al.*, 1993; *Eliasson et al.*, 1994; *Onsager and Mukai*, 1995; *Sauvaud et al.*, 1999]. The flows are commonly equated with a spatial boundary between the central plasma sheet and the tenuous plasma of the two tail lobes, the so called "plasma sheet boundary layer", or PSBL [e.g. *Parks et al.*, 1979; *Eastman et al.*, 1985], and are also referred to as "velocity dispersed ion structures", or VDIS [e.g. *Bosqued et al.*, 1993; *Onsager and Mukai*, 1995].

While interpretations vary somewhat between the different sets of data, ranging from an image of essentially continuous flows [*Lyons and Speiser*, 1982; *Eastman et al.*, 1985; *Onsager et al.*, 1991] to one

of intermittent flows [*Krimigis and Sarris*, 1980; *Spjeldvik and Fritz*,1981; *Williams*, 1981; *Lyons et al.*, 1999; *Sauvaud et al.*, 1999] and a rather complex particle and field environment [*Parks et al.*, 1984], the prevailing view is that these flows are evidence of fundamental magnetotail dynamics. That view is based on one or more of at least three considerations: (1) Flows of a similar kind were predicted prior to observations, based on single-proton dynamics in early models of the tail magnetic and electric fields [*Speiser*, 1965; *Lyons and Speiser*, 1982]; (2) in the presence of strong and steady equatorward **E×B** drift, the observed ion flows, along with earthward flows of electrons, may well serve to populate the near-Earth plasma sheet from the distant tail [*Lyons and Speiser*, 1982; *Eastman et al.*, 1985; *Onsager et al.*, 1991], and (3) they are, in any case, evidence of particle acceleration in the tail [*DeCoster and Frank*, 1979; *Lyons and Speiser*, 1982]. In a superficial sense, at least, these points can be viewed as different aspects of one and the same concept, namely that tail magnetic reconnection is the fundamental process in question [e.g. *Hones et al.*, 1986].

The present study pays yet another visit to this important subject, this time with the help of ion composition data at $E/Q \leq 33$ keV/*e* from the TIMAS instrument on the NASA GGS Polar satellite, launched on February 26, 1996. These data, which treat protons separately from other possibly substantial ionic components (e.g. O^+ ions), have a temporal resolution (seconds) equal to or somewhat better than earlier mixed-ion data and much better than earlier generations of mass-analyzed ion data (minutes). The benefit of the TIMAS data to this specific subject is achieved in large measure by the orbit of the Polar satellite. Being near-polar, the orbit ensures that the TIMAS instrument traverses the plasma sheet-lobe boundary on a regular basis, albeit in its earthward extension, irrespective of geomagnetically controlled boundary motion. With a large apogee ($R \approx 9$ R_E) situated above the north pole (at the time), the orbit also allows the TIMAS to traverse the northern boundary at moderate speed (over the course of multiple s/c spin cycles) and at an altitude sufficiently high ($R \sim 4$-7 R_E) that the atmospheric loss cone is but a small part (a few degrees) of the local ion velocity distributions. The latter allows time-of-flight comparisons between protons of pitch angles α and $180° - \alpha$ over a substantial range of angles. Two representative Polar orbits from the study are illustrated in Figure 1 in solar magnetic (SM) coordinates. The orbital period is 17.63 hours.

The focus here is on the second point listed above, namely the possible role of the proton flows in populating the near-Earth plasma sheet. The specific question to be addressed is the following: Is it true that the characteristic proton velocity dispersion ascribed to the PSBL is a latitudinal one? That is, do the protons usually have their highest energy and most strongly earthward field-aligned pitch-angle distribution at a high-latitude edge of the plasma sheet, becoming gradually less energetic and more isotropic with decreasing latitude within a thin but finite layer? The answer will prove to be "no", but the dispersion features are quite complex at times, and the TIMAS data do raise new questions that are more difficult to answer. Apart from a difference in energy coverage, the present data ($E/Q \leq 33$ keV/*e*) show notable similarities to the tail data (24 keV/*e* $\leq E/Q \leq$ 2 MeV/*e*) presented by *Williams* [1981]. There are also close similarities to the $E/Q \leq 14$ keV/*e* ion composition data recently obtained by the polar orbiting Interball-Auroral satellite at $R \sim 3$ R_E [*Sauvaud et al.*, 1999].

2. The TIMAS Instrument

The Toroidal Imaging Mass-Angle Spectrograph, or TIMAS [*Shelley et al.*, 1995], combines magnetic mass analysis with simultaneous recording of all species (all M/Q) and a nearly omnidirectional field of view. This combination is accomplished by accepting ions within a 10° by nearly 360° wide window and, following the energy selection, magnetically dispersing them in the radial direction on a large annular detector (MCP) with position-sensitive anode. The total field of view scanned over the course of each 6-second Polar spin cycle is 98% of the full 4π. A grossly omnidirectional sampling is achieved after only

half a spin (3 sec) by a combination of 28 detector sectors, but it takes a full spin to fill in gaps in the angular coverage with the help of an elevation phase shift between the leading and trailing sets of 14 sectors each.

The full energy range is 15 eV/*e* to 33 keV/*e*, covered in 28 channels, of which the 14 even-numbered channels are used on even-numbered spins, and the 14 odd-numbered ones on odd spins. Each set of 14 channels is swept 16 times per spin. Hence, the time to sample essentially the entire energy-angle space available for each ion species is 6 seconds (or 3 sec with angular gaps), but it takes 12 seconds (2 spins) to fill in the interleaving energy channels. The instrument is operated in essentially a fixed cycle, continually processing the ion counts into various mass-energy-angle arrays and returning, within the limitations of available telemetry, the same set of arrays, according to a commanded priority order.

The principal data arrays for this study are 6-second (single-spin) energy distributions in each of 208 partially overlapping solid angles (approx. 22.5° by 22.5° each) for each major ion (all corrected by subtraction of separately monitored detector background counts). For the surveying, these are combined into 12-second and 28-energy pairs and displayed in the spectral forms of differential number flux versus energy and time (averaged over all angles) and flux versus pitch angle and time (averaged over some energies). Pitch angles are calculated during ground data processing with magnetic field information from the Polar MFI instrument [*Russell et al.,* 1995].

3. Illustrative Events

3.1. Two Equatorward Crossings of the Plasma Sheet Boundary

The 12-minute segment of differential H^+ and O^+ flux in Figure 2 illustrates two essential aspects of the data. One is the temporal resolution afforded by 12-second (2-spin) averaging; this is for the most part sufficient to expose at least the energy dispersion of the ions (top two panels) and in many cases the pitch-angle dispersion, as well (bottom two panels). In this and other figures to follow, the energy spectra are only displayed for $E/Q \geq 0.9$ keV/*e* in order to emphasize the downflowing ions from the tail. For lower energy, and in this case already at about 2 keV/*e* (~09:34 UT), the flux is usually dominated by upflowing ions from the ionosphere (pitch angles mostly > 90° at the northern boundary). The upflowing ions are essentially eliminated from the bottom two panels by only including $E/Q \geq 3.3$ keV/*e* in the energy-averaged pitch angles. The inherent pitch-angle resolution in these displays, even without energy averaging, is no better than about 20°. The best resolution by the instrument itself, using special arrays (not shown), is about 11°.

The other aspect is the recurrent sense of the ion dispersions: Whenever a distinct trend is discernible, it always shows decreasing energy and (initially) widening pitch-angle distribution as a function of time. When minor ions appear with discernible dispersion, as the O^+ ions do in this case, they arrive with H^+ ions of similar *E/M* (same velocity), or at a time when such H^+ ions would be due in the low-energy extrapolation of their visible trace. The global geomagnetic activity at the time of observation of the ion dispersions is represented by the 3-hour Kp index in the caption of this and following figures. This particular event occurred on a day of persistent activity ($\Sigma Kp = 33$).

A third aspect unique to this figure (only one with two ion species) is the chemical make-up. The number density in the center of the H^+ trace, at 09:33:06 UT, is 0.42 cm^{-3}, whereas the peak O^+ density, at 09:37:13 UT, excluding the upflowing component at lower energy, is 0.07 cm^{-3}, suggesting an O^+/H^+ ratio of about 17% at the source. That is fairly typical of the central plasma sheet during active conditions [*Lennartsson and Shelley,* 1986].

Since the observations in this case are made while the instrument is moving to lower latitude, it can indeed be argued that the dispersions are latitudinal in nature. In fact, a continuous ion source at some fixed downtail location could produce the same dispersion traces at the changing Polar location if the ions

travel earthward through a suitably strong longitudinal electric field, one that is westward and perpendicular to Earth's magnetic field. That kind of argument has been made with similar (mixed ion) observations during prior space missions [e.g. *Eastman et al.,* 1985; *Zelenyi et al.,* 1990; *Onsager et al.,* 1991; *Saito et al.,* 1992; *Bosqued et al.,* 1993; *Onsager and Mukai,* 1995], and it will be reexamined in more detail below. The event in Figure 2 is, however, unusually "clean" as far as the TIMAS data go; typically there are multiple dispersions, often intermingled in a complex manner. A good example of the latter is shown in the top panel of Figure 3, spanning 30 minutes.

This second event has a somewhat larger than normal number of structures, at least a dozen, but it is typical in the sense that few structures span a large range of energy. Several dispersion traces, while tending downward in energy, appear interrupted, either by a flux dropout or by the appearance of a new trace at high energy. In particular, the first, most poleward feature can be made out to consist of at least three closely spaced partial traces with peak flux at increasing initial energy. The narrow (~24 sec) stripe extending downward at 22:32 UT is created by upflowing protons from the ionosphere at energies below 4 keV (peak flux at > 140° pitch angle; not shown).

The fragmented appearance of most dispersion traces in this event, and in others to follow, probably reflects strong spatial inhomogeneities among the ion flows, that is numerous flow filaments, passed across the instrument by plasma convection or satellite motion, or both. This explanation is presaged by the earlier findings of *Spjeldvik and Fritz* [1981] and *Williams* [1981] that earthward ion flows in the tail, at $E/Q > 24$ keV/*e*, may appear in "a layer" of ~2 ion gyro radii thickness. The observations of plasma filaments in the lobes by *Huang et al.* [1987] have similar implications. This aspect of the TIMAS data is intriguing but leads beyond the scope of this initial survey and will be discussed only briefly below.

3.2. Poleward Crossings of the Plasma Sheet Boundary

Being that the Polar is in a near-polar orbit, it is possible to cross from the plasma sheet to the lobe in essentially any state of boundary motion, including that of a stationary boundary. Given a sufficient number of randomly selected poleward crossings, it should therefore be possible to determine whether dispersions of the kind shown in Figure 2 are, at times at least, latitudinal rather than temporal. That is, it should be possible to find some that are reversed in time if latitudinal dispersion spans at least a substantial fraction of 1° and lasts at least a few minutes. This has been the principal motivation for examining well over 100 poleward crossings during the month of October in 1996, 1997 and 1998. The only selection criteria have been (1) to have at least one hour of continuous data coverage for H^+ ions, centered on the plasma sheet-lobe transition region, (2) to have a significant number of crossings, and (3) to focus on a near-midnight local-time sector in the northern hemisphere. The latter two conditions have dictated the choice of time frames.

The middle panel of Figure 3 shows the only type of dispersion found that resembles a time-reversal of Figure 2, that is H^+ energy increasing with increasing latitude through the boundary. There are only a few of this type, and they are not limited to poleward crossings. In fact, the feature of enhanced flux to the right in this panel, adjacent to the lobe, is similar, as a function of time, to the leftmost feature in the panel above. Both appear to consist of three or more closely spaced partial traces with increasing initial energy but otherwise downward sloping leading edge, like the sloping of several other faint traces during this poleward crossing (the bottom feature at 02:51 UT, below 3 keV, again contains upward flowing protons).

This particular and somewhat uncommon type of dispersion is borderline "vague" but is henceforth referred to as "stepping up" in energy, in reference to its apparent multi-component nature. A more common and more genuinely "vague" type of dispersion is illustrated in the bottom panel of Figure 3. This crossing took place on a day of very weak global geomagnetic activity, as defined by the Kp index (ΣKp = 3+), and it does to some extent typify such conditions, although the apparent correlation between

Kp and the rate of occurrence of "distinct" ion dispersion traces is rather marginal (see below).

As a counter point, the upper panel of Figure 4, spanning a full UT hour, shows a crossing during geomagnetically very active conditions (preceding two Kp values were 7- and 7+). In this case there are indeed many distinct, if only partial, downward sloping dispersion traces, spanning some 7° invariant latitude. However, multiple distinct traces may be found during modest global activity, as well, as illustrated by the lower panel of Figure 4, which also spans an hour of Universal Time. This crossing has a fairly smooth and extended trace adjacent to the lobe on the far right, which will be examined in more detail below. The isolated feature centered at 19:35 UT is another example of closely spaced partial traces that are, presumably accidentally, "stepping up" in energy, like the high-latitude "boundary" in the top two panles of Figure 3. In this case it is followed by a series of more extended downward sloping traces at still higher latitude.

4. Statistical Survey

Figures 2 through 4 illustrate 6 out of a total of 142 boundary crossings that were selected on the basis of the three criteria listed above, a total which includes 36 equatorward crossings in April of 1998. Using the spectra of differential number flux versus energy and time as the main tool, the outermost H^+ dispersion trace at the boundary, as observed, was classified according to three categories of sloping: (1) "downward", (2) "stepping up", and (3) "vague". Initially, a fourth category, "upward", was envisioned, but it proved superfluous. The three kinds were defined in the following fashion.

1. Downward:
   - 1.a. Substantial segment of a downward sloping trace, like any of several such traces in for example Figure 4.
   - 1.b. Narrow patch or stripe (~few s/c spins) following a series of distinctly downward traces, like the last pair of stripes (4 spins) in the lower panel of Figure 4. This only applies to poleward crossings and assumes that the last feature is the beginning of another downward trace in the series, one that is interrupted because Polar exits through a sharp plasma boundary.
2. Stepping up:
   Like the poleward boundary in the top two panels of Figure 3.
3. Vague:
   - 3.a. Nearly flat horizontal band (over several minutes) or, like in the bottom panel of Figure 3, rather hazy pattern.
   - 3.b. Similar to poleward boundary in the top two panels of Figure 3 but without upward trend in energy from one patch to the next ("stepping down" trend included).

These, however, still leave some cases to discretion, like the upper panel of Figure 4. The last trace in that event does have a downward sloping leading edge, but it is only faint and rather short. It has nevertheless been classified as "downward", rather than "vague", in part because it forms the end of a long series of downward traces of varying intensity. The statistical results are listed in Table 1, which includes the category label "upward" for emphasis.

4.1. Relation to Global Geomagnetic Activity

The bottom panel in Figure 3 and top panel in Figure 4 show, respectively, the geomagnetically least and most disturbed crossings, but both types of spectral dispersion may be found over a wide range of activity. If the "+" and "-" gradations on the Kp index are given the decimal values of +0.3 and –0.3, respectively, then the linearly averaged Kp from each category of dispersion in Table 1 is as follows:

"Downward" has Kp ≈ 2+, "stepping up" has Kp ≈ 2, and "vague" has Kp ≈ 2-.

5. Generic Velocity Dispersion

As mentioned in conjunction with Figure 2 and amply illustrated in Figures 3 and 4, the proton energy dispersions, while tending downward, are typically interrupted partway, either by flux dropout or by a new dispersion, or new "blast" of protons, starting at higher energy. In Figure 4, however, there is one on the far right in the lower panel, adjacent to the lobe, that has fairly uniform flux and actually does reach the bottom of the display, at 0.9 keV, making it one of the better suited for dissection.

Figure 5 shows contours of constant proton phase space density (above minimum) at four points along that last dispersion trace, each frame representing a 2-spin (12-sec) average ending at the Universal Time labeled "Stop". This figure includes the full velocity range of measured protons and shows therefore also the contours of slower upflowing protons, centered on the negative V_Z-axis.

Figure 5 is generic in that (1) the downflowing (along positive V_Z-axis) protons first appear with significant density (above specified minimum) in a crescent-shaped domain (top left), or dome-shaped in three dimensions, (2) this domain subsequently forms a closed shell (top right), the center of which is offset from zero velocity toward the upflowing (opposite) direction, (3) peak density increases (increasing number of contours; bottom left), and (4) the shell converges toward zero velocity (bottom right). Of these points, number 2 is partially instrumental in that TIMAS is incapable of resolving the few degree wide atmospheric loss cone at the high altitude of these observations. Point 1 is of special significance in that it embodies the reason why these proton flows always appear at first with a large earthward and field-aligned bulk velocity, in this case greater than 1000 km s^{-1}. While changing from 1 to 2 (not shown), the distribution briefly takes a shape that may be likened to a "horseshoe" (cf. Figure 3b in *Eliasson et al.* [1994]).

In gross kinematic terms, this kind of dispersion fits a rather simple mold, as illustrated in Figure 6. Here, the converging oval-shaped (solid) curves may be viewed as the succesive location in velocity space of the leading edge on a population of protons that is suddenly released from R_0 at time $t = 0$ with wide ranges of speed (extending at least to 2500 km s^{-1}) and pitch-angle (earthward), assuming that those protons are only acted upon by the magnetic force $e\mathbf{v}\times\mathbf{B}$. Any pair of ovals with time labels t_1 and t_2 ($> t_1$) may be viewed as the boundaries on such a population when the source is turned off again at time $t = t_2 - t_1$. If the protons are released with an isotropic velocity distribution $f(v)$, that is isotropic over a sufficiently large earthward range of pitch angle $\alpha \geq 0°$, and f has a negative slope, $df/dv < 0$, then the condition $f(v) >$ some minimum value at the Polar position will first be met within a crescent-shaped domain, as indicated by the shaded area in the middle panel, assuming that $f(v)$, i.e. the phase space density, is preserved at constant value of v. Of the three cases illustrated here, the middle one most closely approximates the leading edge time sequence (innermost contour) in Figure 5. The "trailing edge" does not follow this simple time-of-flight pattern, however; it indicates a fading source, rather than a turn-off.

The solid contours in Figure 6 have been derived by finding, in a numerical fashion, the minimum speed v required for a proton to reach the Polar position with a given pitch angle α_{obs} within a given time t, assuming that its energy and magnetic moment are preserved, that is

$$v^2 = v_{obs}^2 \qquad (1)$$

$$\sin^2 \alpha \cdot B^{-1} = \sin^2 \alpha_{obs} \cdot B_{obs}^{-1} \qquad (2)$$

where "obs" refers to the point of observation. The magnetic field line through the Polar position (in SM coordinates) is modeled in accordance with *Tsyganenko* [1987] for the nominal epoch (~ 20:00 UT on this day) and magnetic activity (Kp ~ 2). This statistically averaged model is not assumed to reproduce

the specific local conditions well, but it is sufficient to illustrate the gross proton flight times. Those depend mostly on the grand scale size, and the main requirement here is that the model field line reaches sufficiently far downtail in each case. By comparison, the flight times obtained by assuming, for example, simple radial motion and a local field strength $B(R) = 58000\ \text{nT} \times R^{-3} \cdot R_E^3$ while > 10 nT, and $B = 10$ nT beyond, are shorter but differ less than 10% from those in the middle panel of Figure 6.

6. Discussion

In the perspective of the TIMAS instrument, at $R \sim 4\text{-}7\ R_E$, the earthward proton flows appear as sudden "blasts" of particles overtaking the Polar satellite as it is moving from a plasma sheet-like environment to a low-density near-Earth lobe, or moving in the opposite (equatorward) sense. Many events appear spatially separated from the plasma sheet, sometimes occurring during conditions of near vacuum, as in the lower panel of Figure 4, beginning and ending virtually instantaneously, that is faster than the 12-second averaging of the data and substantially faster than the proton energy dispersion.

Some abrupt changes in proton flux, from one 12-second sampling to the next, are found during all crossings of the plasma sheet boundary, if not always by orders of magnitude, as in Figure 4. This phenomenon may well be a fundamental physical aspect of the proton "blasts", but it appears somewhat separate from the energy and pitch-angle dispersions in the data, suggesting that the instrument often encounters sharp spatial flux gradients in addition to the temporal effects. For a brief analysis of this aspect, consider again the last couple of dispersion traces in Figure 4, in particular the one dissected in Figure 5.

As Polar passes through the last 4-minute dispersion feature in Figure 4, bottom, moving northward, nearly perpendicular to Earth's magnetic field (top left panel in Figure 1), at about 2.6 km s^{-1}, the measured magnetic field strength B [*Russell et al.,* 1995] varies from 184 nT (low proton flux) to a minimum of 179 nT (~ peak proton flux) and back to 183 nT (in lobe). With, for example, $B \approx 181$ nT representing interior conditions near the edges, one thus obtains local proton gyroradii, at 90° pitch angle, between 24 km and 145 km over the energy range of Figure 4, with an average of about 80 km. By comparison, Polar travels 2.6 km $s^{-1} \times 12$ s ≈ 31 km during each 2-spin TIMAS sampling. Hence, the observed abrupt changes in flux cannot be well explained by the satellite motion alone, even if the gradients are defined at the gyro radii level; they imply somewhat faster motion of the flow filaments themselves, by **E×B** drift. It may be mentioned that the local change in B, from 184 to 179 nT, corresponds fairly well, in the diamagnetic sense, to the measured proton density n_p at about 19:59 UT (above 0.9 keV) and the associated mean proton energy $m_p\langle v^2\rangle 2^{-1}$, assuming rough isotropy (cf. lower left panel in Figure 5). Those two numbers, which are relevant to the following discussion, are $n_p \approx 0.55$ cm^{-3} and $m_p\langle v^2\rangle 2^{-1} \approx 8$ keV, respectively.

Spin-by-spin examination of the raw data matrices (not shown) through the last few dispersions in Figure 4, bottom, reveals that the sharp flux edges are indeed coincident with strongly nonuniform distribution of counts over solid angle, as would be expected with large spatial gradients on the length of a proton gyroradius [cf. *Spjeldvik and Fritz,* 1981; *Williams,* 1981; *Huang et al.;* 1987]. Somewhat surprisingly, perhaps, these gradients appear at this time to be longitudinal, i.e. in the dawn-dusk direction, rather than latitudinal. For example, the sudden end of the next to last dispersion, at about 19:57 UT, coincides with a well defined dropout of protons that would have had their gyrocenters on the dawnside of Polar, indicating a rapid (> 10 km s^{-1}) duskward displacement of the whole flow structure. In reference to the earlier, patchy structure about 19:35 UT, which is only seen at high energies, it is worth noting that if Polar skims the outer edge of a flow filament, the largest gyroradii (highest energies) may be the only ones intersecting the instrument. That same note applies to the "stepping up" boundary features in Figure 3 as well. A quantitative discussion of these effects will have to await the development of a suitable

two-dimensional TIMAS angular display, however.

While it is obvious that protons (and other ions) must flow along magnetic field lines in order to reach Polar from the tail, there is no evidence in the TIMAS data that the proton velocity distribution is inherently field-aligned at the source. By the time the protons reach down to the Polar altitude, their "field-alignment" is transient, the main effect lasting a mere minute or so, and fits the gross time-of-flight pattern of Figures 5 and 6. In general, the TIMAS data would look identical if the proton "blast" at $t = 0$ were isotropic.

The 4π at Polar does of course correspond to a much smaller solid angle $\delta\Omega$ at the downtail source, easily by two orders of magnitude if that is in the tail midplane at, say, $R \sim 30\ R_E$ (e.g. if source has $B =$ 7 nT in Figure 5), but the maximum proton density in the dispersion traces (about where the differential flux peaks) is typically in the range $n_p \sim 0.1\text{-}0.5\ cm^{-3}$ (the last trace in Figure 4 has one of the highest densities), so filling the 4π at the source uniformly with the same phase space density would yield a proton number density that merely falls within normal central plasma sheet values [e.g. *Lennartsson and Shelley,* 1986; *Huang and Frank,* 1986; *Baumjohann et al.,* 1989]. Conversely, if a midplane source about $30\ R_E$ downtail were indeed limited to $\sim \delta\Omega$ in angular space, then it would have a number density far smaller than (~1% of) the normal ambient plasma sheet population. In either case, the central plasma sheet is probably a sufficient material source for the dispersed protons observed by TIMAS.

The largest differential number flux ($\sim 10^6$) among the proton energy dispersions is usually found in the 4-12 keV range, even when the trace extends below 4 keV (e.g. last one in Figure 4). This statistical range may be compared to the parametric energy where an isotropic Maxwell-Boltzmann distribution has its peak flux, namely the thermal energy kT. Although the dynamic nature of the dispersions makes this a crude comparison, it does suggest that the dispersed protons have a "temperature" which is similar to what central plasma sheet protons have during moderately to strongly disturbed geomagnetic conditions [*Huang and Frank,* 1986; *Baumjohann et al.,* 1989; *Huang et al.,* 1992] but significantly higher than that of central plasma sheet protons during extended periods of magnetic quiescence (~1 keV; see *Lennartsson and Shelley* [1986]; *Fujimoto et al.* [1997]; see also bottom panel of Figure 3 above). Since many of the dispersions do occur during rather quiet conditions, as measured by the global Kp index (bringing down the "downward" average in Section 4.1), it seems probable that their elevated bulk energy is generated during the "blast" itself (e.g. by electromagnetic induction; cf *Huang et al.* [1992]).

Extending that line of reasoning to globally active conditions, one may speculate that the central plasma sheet then shows the cumulative effect of widespread "blasting", especially near local midnight, since its temperature peaks there [*Lennartsson and Shelley,* 1986]. Indeed, the upper panel of Figure 4, representing strongly disturbed conditions, has many dispersions spanning some 7° invariant latitude, and the slope of the dispersions varies somewhat randomly, as though a large radial range of the near-midnight (~00:10 MLT) tail is active concurrently.

As far as the "generic" velocity dispersion in Figure 5 is concerned, having substantial acceleration in the course of transit means that Equation 1 (at least) is inaccurate and that the distance traveled may be shorter than the estimate in the middle panel of Figure 6 (lower average speed). In other words, the proton source may well be less than $30\ R_E$ downtail in this case, and substantially less in many other cases, since the dispersion traces are often steeper (e.g. some in the upper panel of Figure 4; see also *Sauvaud et al.* [1999]).

6.1. Possible Diamagnetic Mechanism

Among the various aspects in need of an explanation are thus (1) the high-latitude occurrence of the proton flows, sometimes well outside of the plasma sheet, (2) the often close (apparent) location of the proton source, less than $30\ R_E$ downtail in many cases, (3) the sudden onset of (weak) flux at high energy, followed by (stronger) flux at decreasing energy, (4) the typically plasma sheet-like peak flux levels, and

(5) the transient (~few minutes), "blast-like" nature and (6) common filamentary appearance of the flows.

If one assumes that the source is in or near the tail equatorial plane, 1 and 2 together imply that the protons often flow along magnetic field lines that have a more "dipolar" shape (though not dipolar in terms of field magnitude) than the normal tail field lines. In particular, the $R \sim 30$ R_E estimate from Figures 5 and 6 is less than halfway to the equatorial crossing point ($R = 72$ R_E) of the model magnetic field line [*Tsyganenko,* 1987] through the point of observation.

Number 4 makes it plausible, if not certain, that the source is indeed near the equatorial plane, rather than in the low-density plasma at high latitude. Numbers 3 and 5 suggest that the central plasma sheet is only intermittently connected to higher latitude, presumably locally, and 6 is perhaps direct evidence of localized connections.

These aspects can be synthesized in a descriptive physical sense by invoking the diamagnetic properties of the plasma sheet. That is, if one envisions that the equatorial plasma pressure becomes slightly reduced at some point, for whatever reason, its normal balance with the adjacent lobe magnetic field [*Fairfield et al.,* 1981] is interrupted, and some higher-latitude field lines can "reroute themselves" through the nearby equatorial plane, that is "dipolarize" locally, and reduce their potential energy. The altered field topology in turn allows the equatorial plasma to expand earthward along "new" field lines to higher latitude, where the plasma pressure is lower still, and thereby reinforce this change in field topology.

This synthesis is executed in more detail in *Lennartsson* [1997] with ion composition data from the ISEE 1 satellite, including a schematic drawing (Figure 5 there). The context in that case is the plasma sheet "thinning" and "recovery" sequence during substorms [*Hones et al.,* 1971].

The "variable nature of the source" of earthward proton (ion) flows was already noted by *Williams* [1981] during a 16-hour interval of ISEE 1 observations in the tail, and he attributed it to either (a) "a time variable source", (b) "a spatially moving source", or (c) "random encounters of the ISEE 1 flux tube with a steady source". His observations have essentially the same aspects as those listed above, with the possible exception of 2. At the time the ISEE 1 satellite was located at R ~16-22 R_E in the dusk-midnight quadrant, and the source was inferred to be as much as 60-80 R_E further downtail. Number 4 still applies, however, since the observed flux peaks at 10^4-10^5 $(cm^2\ s\ ster\ keV)^{-1}$ at 24 keV (low end) and falls rapidly with increasing energy (Figures 5 and 6 in that paper). This is consistent, within the substantial range of temporal variations, with a high-energy tail on the TIMAS flux. The third, c, of Williams' proposed explanations is the one that most literally foreshadows the present synthesis.

6.2. Bearing on Neutral Line

This "diamagnetic scenario" does not necessarily call for a "neutral line" in the customary sense of MHD [e.g. *Cowley,* 1980], nor do the data themselves. In fact, such a feature, when immersed in a westward longitudinal electric field **E** (parallel to the line),would create true latitudinal dispersion, always in the directional sense of Figure 2, in conflict with the TIMAS observations. The reason is, of course, that the plasma convects across that line in a manner of a "conveyer belt" passing a station where the ions are locally accelerated in the direction of **E** (and subsequently deflected earthward by the magnetic field [*Speiser,* 1965]).

For a crude quantitative consideration, see again the top panel of Figure 2. It shows a proton energy dispersion taking place across 0.7° invariant latitude, that is across some 80 km horizontal distance at ionospheric altitude (at 100 km altitude). The field-aligned velocites of the most energetic (33 keV) and least energetic (~3 keV) of these protons, at 0° pitch angle, are about 2500 km s^{-1} and 760 km s^{-1}, respectively. If a neutral line were located, say, 100 R_E downtail, the differential flight time of those protons from there to the Polar position would be about 10 minutes, a time during which they could be separated in latitude. Hence, in terms of **E**×**B** drift, this corresponds to a very modest 0.1 km s^{-1} at iono-

spheric altitude (80 km in 10 min) and, in terms of the convection electric field, only about 7 mV m^{-1}. With the neutral line as close as 50 R_E downtail, the corresponding numbers would still be quite modest, namely 0.3 km s^{-1} for the convection speed and 16 mV m^{-1} for the electric field. These low-altitude reference numbers demonstrate, indirectly, that a neutral line at "ordinary" distance downtail would indeed create measurable latitudinal dispersion in the TIMAS data (like in Figure 2) if it were to remain stationary for at least some 10 minutes, and provided it were capable of imparting the observed range of proton energies (~30 keV).

The absence of latitudinal dispersion in the TIMAS data can be reconciled, however, with a transient, near-equatorial plasma source which itself travels with the **E×B** drift and occupies the cross section of a finite magnetic flux tube. What is seen at Polar then depends on whether the satellite is inside or outside the flux tube following the source turn-on (i.e. after the local magnetic field starts to dipolarize). Being already inside means seeing the start of the ion dispersion, and if entering or leaving, the direction of cross-field motion does not affect the sense of ion dispersion. Besides, motion relative to the flux tube is likely to be controlled by plasma **E×B** drift rather than by latitudinal satellite motion (see beginning of this section).

It could perhaps be argued that such drifting plasma structures are launched by short-lived and/or moving near-Earth neutral lines, but that would still leave unanswered the question how the expanding plasma finds its way outside the plasma sheet by the time it reaches Polar altitudes. In any case, there is the larger issue of whether a fluid description is appropriate in the first place. As pointed out above, but discussed only briefly, the TIMAS data show evidence that spatial scales as small as proton gyroradii are involved (see also *Spjeldvik and Fritz* [1981]; *Williams* [1981]; *Huang et al.* [1987]), and this does bring into question the validity of MHD in this context.

7. Conclusions

The answer to the specific question posed in the introduction (last paragraph) must be "no"; the proton (and other ion) velocity dispersions in the TIMAS data, when discernible, are by all indications temporal in nature, and there is no consistent latitudinal dispersion per se. This is not to say that our customary vision of persistent equatorward plasma convection in the near-midnight auroral regions must be wrong; the implication is rather that the ions are arriving from a newly "opened" plasma source which is itself convecting. Regardless of what actually does trigger the plasma flows, the present data allow the following conclusions:

1. Proton velocity dispersions are temporal ("blast-like") rather than latitudinal.

2. Initially strong "field-alignment" of proton velocity distribution is a time-of-flight effect.

3. Dispersions are often steep enough for proton source to be at most a few tens of R_E downtail.

4. Intensity and energy of proton flows are largely consistent with a central plasma sheet source, the energy at peak differential flux being typical of (locally) disturbed conditions (4-12 keV).

5. Flows often have filamentary structure with minimum scale size as small as proton gyroradii.

6. Flows may reach well poleward of (pre-existing) plasma sheet near Earth.

These sundry aspects, taken together, do not mesh well with the notion that the near-Earth plasma sheet

is fed by the field-aligned proton flows; they rather suggest some instability in the diamagnetic confinement of the plasma sheet, perhaps some kind of exchange instability [c.f. *Longmire*, 1963, pp. 241-262]. As far as the supply issue is concerned, there are certainly other possible modes of plasma transport in the tail [e.g. *Lennartsson*, 1997, and references therein].

Acknowledgments. The authors wish to thank J.B. Cladis for the use of his computer code for magnetic field line tracing. This work was supported by NASA under contract NAS5-30302 and grant NAG5-7463.

References

Baumjohann, W., G. Paschmann, and C.A. Cattell, Average plasma properties in the central plasma sheet, *J. Geophys. Res., 94*, 6597, 1989.

Bosqued, J.M., M. Ashour-Abdalla, M. El Alaoui, L.M. Zelenyi, and A. Berthelier, AUREOL-3 observations of new boundaries in the auroral ion precipitation, *Geophys. Res. Lett., 20*, 1203, 1993.

Cowley, S.W.H., Plasma populations in a simple open model magnetosphere, *Space Sci. Rev., 26*, 217, 1980.

DeCoster, R.J., and L.A. Frank, Observations pertaining to the dynamics of the plasma sheet, *J. Geophys. Res., 84*, 5099, 1979.

Eastman, T.E., L.A. Frank, and C.Y. Huang, The boundary layers as the primary transport regions of the Earth's magnetotail, *J. Geophys. Res., 90*, 9541, 1985.

Eliasson, L., *et al.*, Freja observations of heating and precipitation of positive ions, *Geophys. Res. Lett., 21*, 1911, 1994.

Fairfield, D.H., R.P. Lepping, E.W. Hones, Jr., S.J. Bame, and J.R. Asbridge, Simultaneous measurements of magnetotail dynamics by IMP spacecraft, *J. Geophys. Res., 86*, 1396, 1981.

Fujimoto, M., T. Terasawa, and T. Mukai, The cold-dense plasma sheet: A GEOTAIL perspective, *Space Sci. Rev., 80*, 325, 1997.

Hones, E.W., Jr., J.R. Asbridge, and S.J. Bame, Time variations of the magnetotail plasma sheet at 18 R_E determined from concurrent observations by a pair of Vela satellites, *J. Geophys. Res., 76*, 4402, 1971.

Hones, E.W., Jr., T.A. Fritz, J. Birn, J. Cooney, and S.J. Bame, Detailed observations of the plasma sheet during a substorm on April 24, 1979, *J. Geophys. Res., 91*, 6845, 1986.

Huang, C.Y., and L.A. Frank, A statistical study of the central plasma sheet: implications for substorm models, *Geophys. Res. Lett., 13*, 652, 1986.

Huang, C.Y., L.A. Frank, W.K. Peterson, D.J. Williams, W. Lennartsson, D.G. Mitchell, R.C. Elphic, and C.T. Russell, Filamentary structures in the magnetotail lobes, *J. Geophys. Res., 92*, 2349, 1987.

Huang, C.Y., L.A. Frank, G. Rostoker, J. Fennell, and D.G. Mitchell, Nonadiabatic heating of the central plasma sheet at substorm onset, *J. Geophys. Res., 97*, 1481, 1992.

Hultqvist, B., H. Borg, W. Riedler, and P. Christophersen, Observations of magnetic-field aligned anisotropy for 1 and 6 keV positive ions in the upper ionosphere, *Planet. Space Sci., 19*, 279, 1971.

Krimigis, S.M., and E.T. Sarris, Energetic particle bursts in the earth's magnetotail, in *Dynamics of the Magnetosphere*, edited by S.-I. Akasofu, p. 599, D. Reidel, Hingham, Mass., 1980.

Lennartsson, O.W., ISEE ion composition data with implications for solar wind entry into Earth's magnetotail, *Space Sci. Rev., 80*, 305, 1997.

Lennartsson, W., and E.G. Shelley, Survey of 0.1- to 16-keV/*e* plasma sheet ion composition, *J. Geophys. Res., 91*, 3061, 1986.

Longmire, C.L., *Elementary Plasma Physics*, John Wiley, New York, 1963.

Lui, A.T.Y., E.W. Hones, Jr., F. Yasuhara, S.-I. Akasofu, and S.J. Bame, Magnetotail plasma flow during plasma sheet expansions: Vela 5 and 6 and IMP 6 observations, *J. Geophys. Res., 82*, 1235, 1977.

Lyons, L.R., and T.W. Speiser, Evidence for current sheet acceleration in the geomagnetic tail, *J. Geophys. Res.*, 87, 2276, 1982.

Lyons, L.R., T. Nagai, G.T. Blanchard, J.C. Samson, T. Yamamoto, T. Mukai, A. Nishida, and S. Kokubun, Association between Geotail plasma flows and auroral poleward boundary intensifications observed by CANOPUS photometers, *J. Geophys. Res., 104,* 4485, 1999.

Onsager, T.G., and T. Mukai, Low altitude signature of the plasma sheet boundary layer: Observations and model, *Geophys. Res. Lett., 22,* 855, 1995.

Onsager, T.G., M.F. Thomsen, R.C. Elphic, and J.T. Gosling, Model of electron and ion distributions in the plasma sheet boundary layer, *J. Geophys. Res., 96,* 20999, 1991.

Parks, G.K., C.S. Lin, K.A. Anderson, R.P. Lin, and H. Reme, ISEE 1 and 2 particle observations of outer plasma sheet boundary, *J. Geophys. Res., 84,* 6471, 1979.

Parks, G.K., *et al.,* Particle and field characteristics of the high-latitude plasma sheet boundary layer, *J. Geophys. Res., 89,* 8885, 1984.

Paterson, W.R., L.A. Frank, S. Kokubun, and T. Yamamoto, Geotail survey of ion flow in the plasma sheet: observations between 10 and 50 R_E, *J. Geophys. Res., 103,* 11,811, 1998.

Russell, C.T., *et al.,* The GGS/Polar magnetic fields investigation, in *The Global Geospace Mission,* ed. by C.T. Russell, Kluwer Academic Publishers, Dordrecht, 563, 1995.

Saito, Y., T. Mukai, M. Hirahara, S. Machida, and N. Kaya, Distribution function of precipitating ion beams with velocity dispersion observed near the poleward edge of the nightside auroral oval, *Geophys. Res. Lett., 19,* 2155, 1992.

Sauvaud, J.-A., *et al.*, Sporadic plasma sheet ion injections into the high altitude auroral bulge - Satellite observations, *J. Geophys. Res., 104,* 28,565, 1999.

Shelley, E.G., *et al.,* The toroidal imaging mass-angle spectrograph (TIMAS) for the Polar Mission, in *The Global Geospace Mission,* ed. by C.T. Russell, Kluwer Academic Publishers, Dordrecht, 497, 1995.

Speiser, T.W., Particle trajectories in model current sheets, 1. Analytical solutions, *J. Geophys. Res.,* 70, 4219, 1965.

Spjeldvik, W.N., and T.A. Fritz, Energetic ion and electron observations of the geomagnetic plasma sheet boundary layer: three-dimensional results from Isee 1, *J. Geophys. Res., 86,* 2480, 1981.

Tsyganenko, N.A., Global quantitative models of the geomagnetic field in the cislunar magnetosphere for different disturbance levels, *Planet. Space Sci., 35,* 1347, 1987.

Williams, D.J., Energetic ion beams at the edge of the plasma sheet: ISEE 1 observations plus a simple explanatory model, *J. Geophys. Res., 86,* 5507, 1981.

Zelenyi, L.M., R.A. Kovrazkhin, and J.M. Bosqued, Velocity-dispersed ion beams in the nightside auroral zone: AUREOL 3 observations, *J. Geophys. Res., 95,* 12,119, 1990.

O.W. Lennartsson, Lockheed Martin Missiles & Space, ATC,
Org. L9-42, Building 255, 3251 Hanover Street, Palo Alto, CA 94304.
(e-mail: lenn@spasci.com)

Table 1. Slope of H^+ Energy Dispersion Versus Time at Plasma Sheet High-Latitude Boundary

Period	Crossing	No. slope occurrences			
		downward	vague*	"stepping up"	upward
Oct '96	poleward	21	12	1	0
Oct '97	poleward	25	11	2	0
Oct '98	poleward	20	12	2	0
Apr '98	equatorward	21	13	2	0
		$\Sigma = 87$	48	7	0

Total no. crossings: 142

*includes "stepping down"

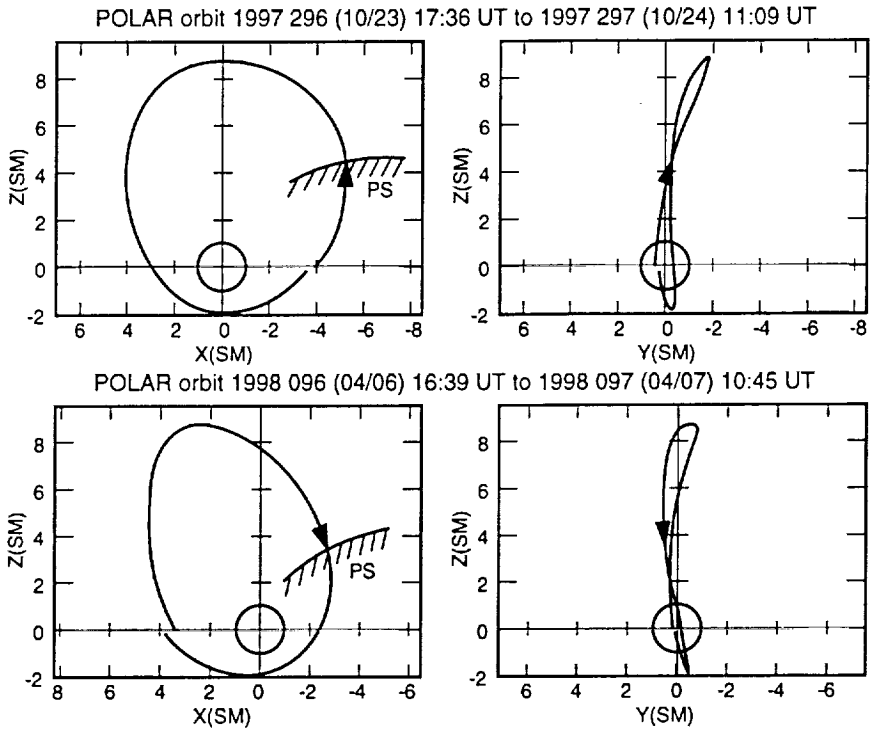

Figure 1. Sample Polar orbits in solar magnetic (SM) coordinates showing (top left) poleward (October) and (bottom left) equatorward (April) crossings of the plasma sheet-lobe boundary close to local midnight (right panels; adapted from *peredo@nssdca.gsfc.nasa.gov*).

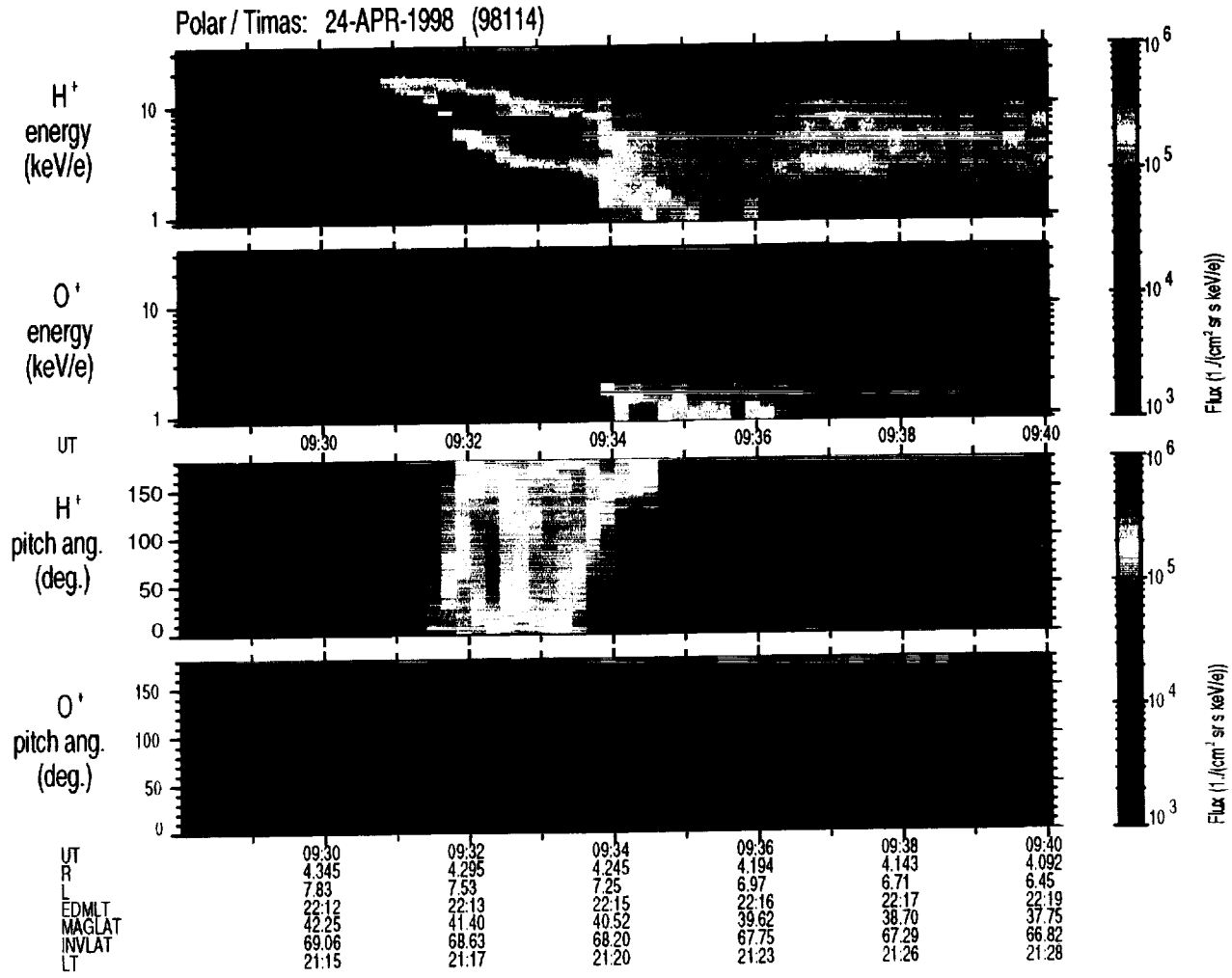

Figure 2. (top) Proton differential number flux (color code to the right) averaged over view angles ($\approx 4\pi$) as function of Universal Time (UT; x-axis) and energy (y-axis) during an equatorward boundary crossing with Kp = 5-. (second) Same for singly charged oxygen ions. (third) Proton flux averaged over energy at $E \geq 3.3$ keV as function of UT and pitch angle. (fourth) Same for oxygen ions. Selected ephemeris data at bottom.

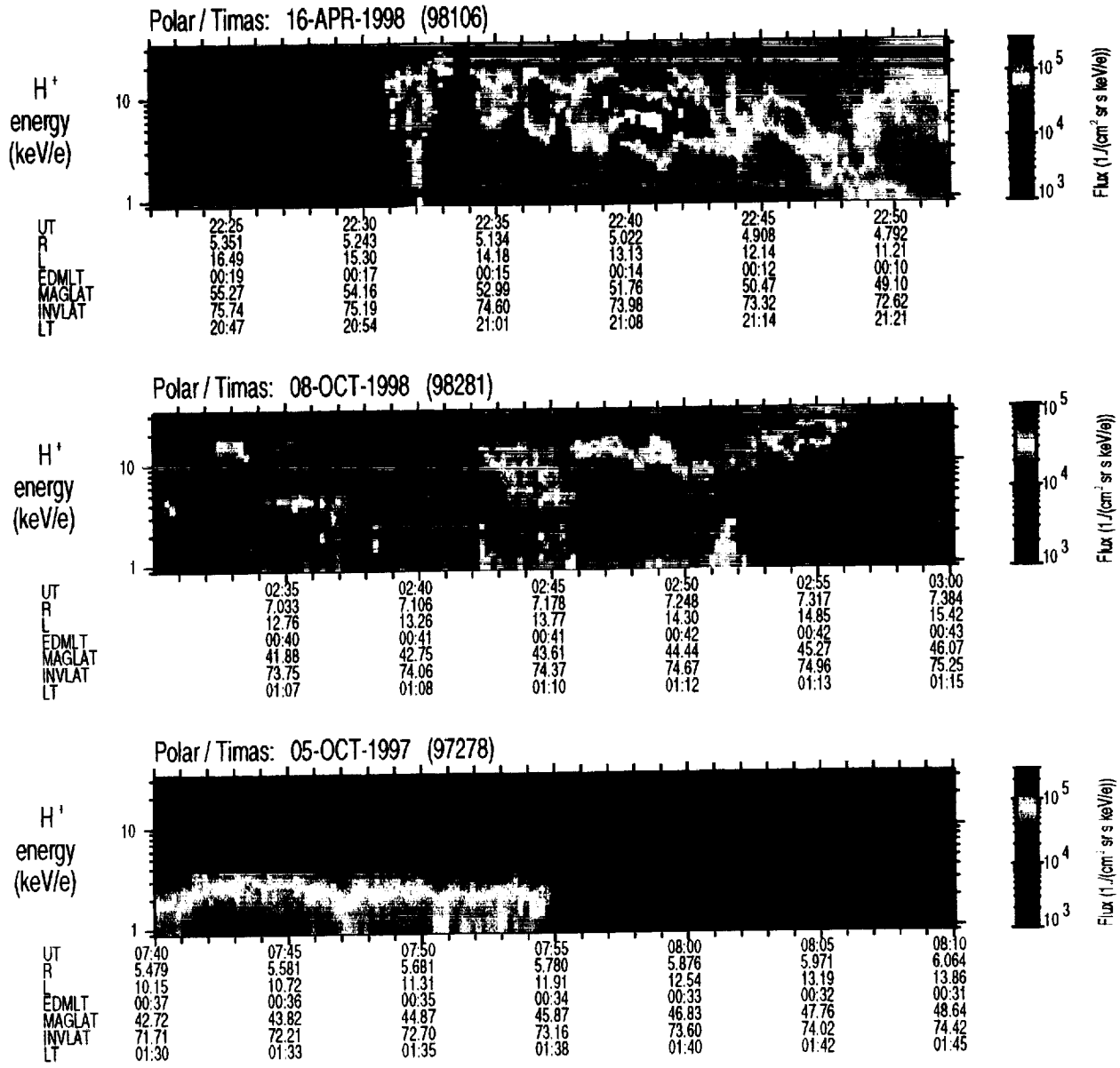

Figure 3. Same format as top panel of Figure 2 but spanning 30 minutes of Universal Time. (top) Equatorward crossing with Kp = 3-. (middle) Poleward crossing with Kp = 4+. (bottom) Poleward crossing with Kp = 0.

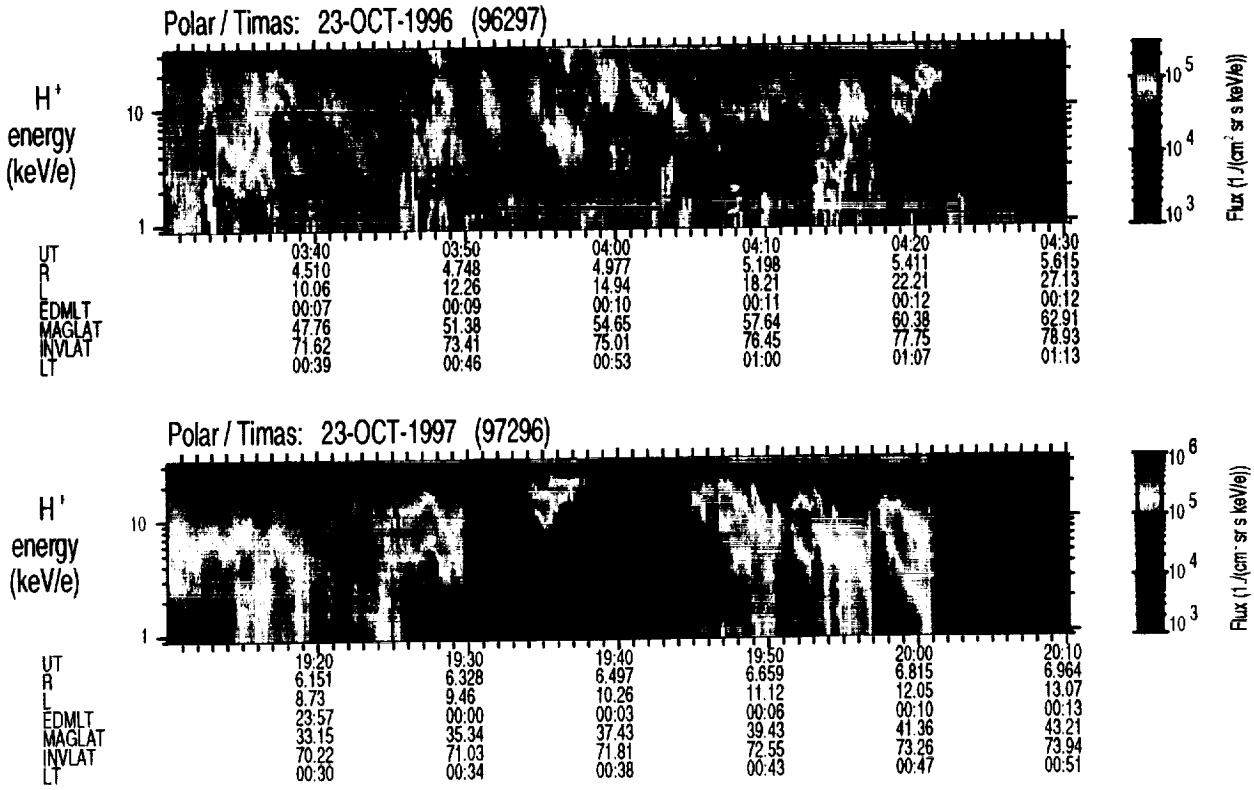

Figure 4. Same format as Figure 3 but spanning 1 hour of Universal Time. (top) Poleward crossing with Kp = 6-. (bottom) Poleward crossing with Kp = 2+.

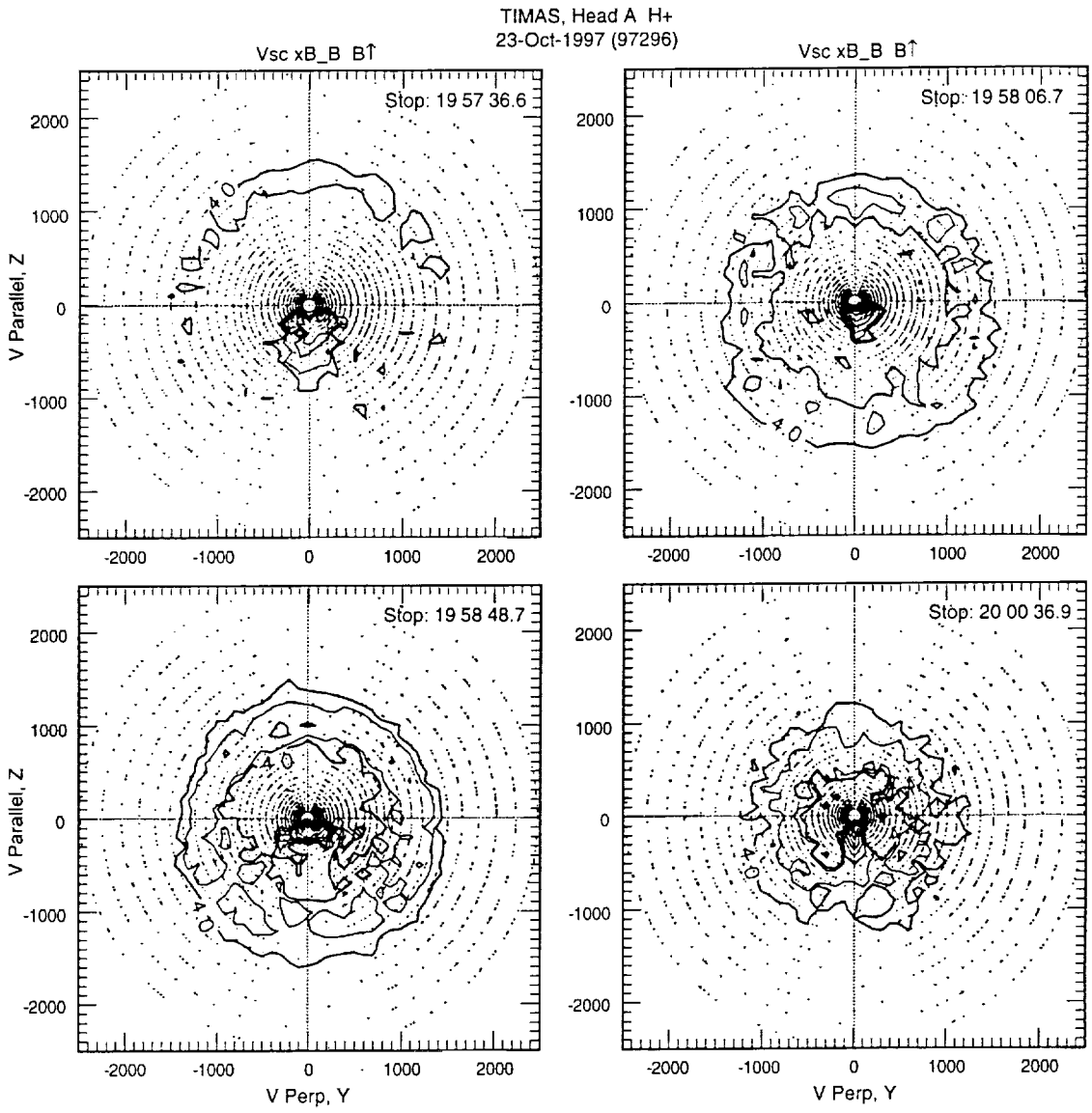

Figure 5. Contours of constant phase space density $f(v_\perp, v_\parallel)$ at four times (labeled "stop") along the last dispersion trace in bottom panel of Figure 4. Units are km s^{-1} for velocity and s^3 km^{-6} for f. Contours are drawn twice per decade where $f \geq 10^4$. Note: the atmospheric loss cone at this altitude ($R \approx 6.8$ R_E) is too small (~3°) to be resolved by instrument (see text for details).

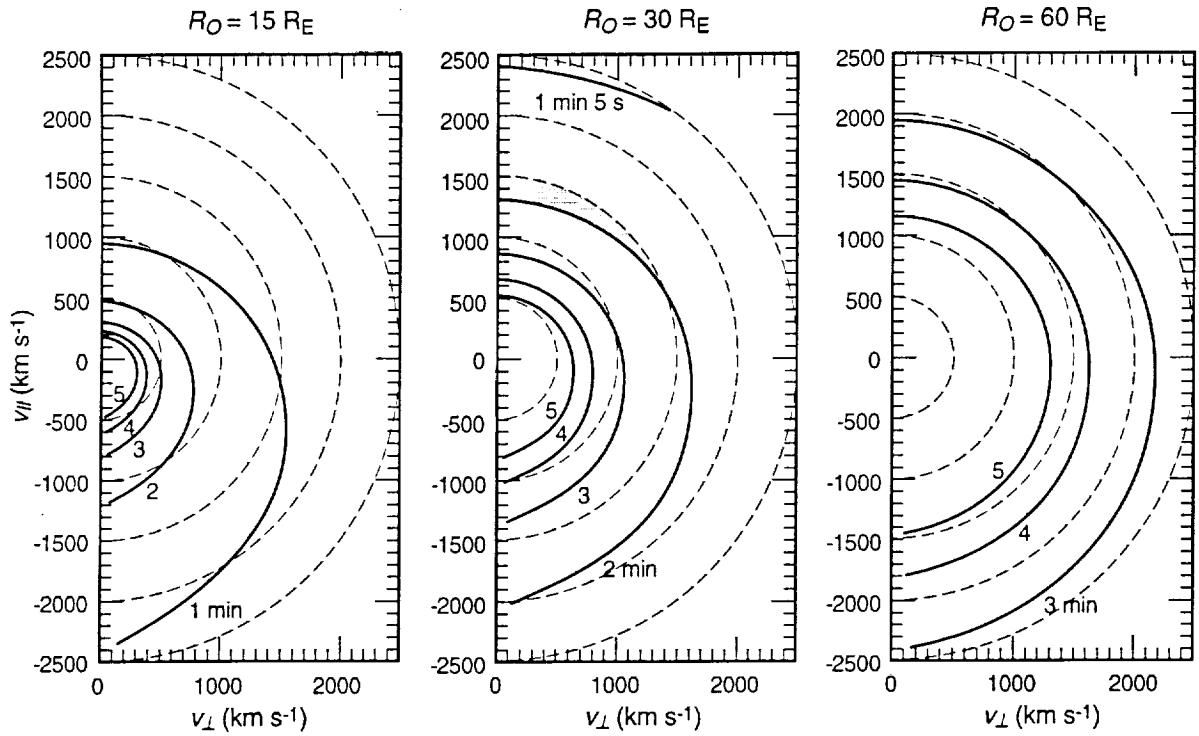

Figure 6. Contours (solid lines) of constant proton time of flight along model magnetic field line from a point at $R = R_0$ downtail to the position of Polar at about the time the data in Figure 5 were acquired. Shaded area in middle panel indicates how approaching proton population is expected to emerge with f exceeding some preset limit when f is isotropic, $f(v_\perp, v_{||}) = f(v)$, and $df/dv < 0$ (see text).